

Analysis of different geophysical methods in the detection of an underground opening at a controlled test site

Christos Orfanos^{1*} and George Apostolopoulos^{1#}

¹National Technical University of Athens, School of Mining and Metallurgical Engineering, Zografou Campus, 15780 Athens, Greece

(*orf@metal.ntua.gr, #gapo@metal.ntua.gr)

(Received 03 October 2011; accepted 25 January 2012)

Abstract: *This study involves the application and the analysis of four geophysical methods (resistivity tomography, microgravity, magnetic, M.A.S.W.) for the detection of a tunnel under controlled site conditions. Resistivity tomography provided satisfactory information both for the target and the near surface geological formations. Dipole-Dipole and Pole-Dipole are the most suitable arrays for the detection of the investigated void, especially when the later combines forward and reversed measurements. The time consuming and laborious microgravity method is suitable for the delineation of the tunnel. Prior information is necessary for the inversion of the microgravity data. The pseudo-section deduced from Multi-channel Analysis of Surface Waves showed two geological layers and imaged a shallow smoothed heterogeneity, attributed to the underground target. However, the target limits are not well defined due to the low lateral resolution. The gradient magnetic method accurately delineates the tunnel due to the increased magnetic susceptibility contrast between the target and the host rock. This condition is usually satisfied when the target is a contemporary man made structure.*

Key words: Resistivity tomography, microgravity, magnetics, M.A.S.W., tunnel

INTRODUCTION

Cavities, voids, abandoned mine workings and any kind of underground opening can be hazardous in geotechnical and environmental applications or can be the target of an archaeological survey. Geophysical methods provide economic, non destructive and rapid tools for the detection of such targets. There are numerous case studies all over the world showing the effectiveness of geophysical methods in the detection of underground openings. (Sheets and Munk, 1997; Johnson, 2003; Yule et al., 1997; Butler et al., 1984; Hinze, 1990; Branston et al., 2006; Styles et al., 2006; Rybakov et al., 2005; Orfanos et al., 2008).

Firstly, resistivity methods can be very effective in locating underground openings which exhibit a significantly higher resistivity than the host rock. The detection of underground voids in Ohio using resistivity tomography (Sheets and Munk, 1997) and the detection of abandoned mine workings at Regency park Subdivision in Pennsylvania (Johnson, 2003) are typical examples. Microgravimetry is usually employed for detecting and delineating underground openings (Butler, 1980, Yule et al., 1997; Butler et al., 1984; Hinze, 1990; Kis et al., 2005; Branston et

al., 2006, Styles et al., 2006; Kaufmann and DeHan, 2007). Rybakov and Rotstein (2005) showed the capability of the magnetic method in void detection. Compared with other methods, the magnetometry is faster, covering large areas in a short time. Moreover, many researchers have recently been studying the efficiency of the M.A.S.W. in the detection of lateral heterogeneities (Xia et al., 2000, Nasser, 2006).

On the other hand, the main disadvantage of the geophysical methods is the uncertainty of the final interpretation which necessitates verification with direct methods such as drillings. Applying a multitude of geophysical methods reduces this uncertainty to some degree. Of course, even in an integrated geophysical survey, the reliability of the geophysical images greatly depends on the correct and optimized application of each method.

Different factors such as the geological conditions, the type of the target (man made or physical void), the size and the depth of the target, surface relief, can decisively affect the successful application of each method. Moreover, there are three crucial steps that influence the effectiveness of the geophysical survey: a) the acquisition strategy, b) the processing of the measurements and c) the interpretation.

This study presents the application of four geophysical methods (resistivity tomography, microgravity, magnetic, M.A.S.W.) over a known target under controlled site conditions and the comparison of these methods regarding their capability to detect underground confined bodies as well as the quality of the geophysical images.

THE TEST SITE

The survey area is located on the Campus of the National Technical University of Athens. The target is a tunnel (cut and cover) with power and network cables. The presence of a hatch in the surface allows direct measurement of the tunnel's dimensions (Fig. 1a). The tunnel is 2 m high and 3 m wide. The top of the tunnel is located at a depth of approximately 2 to 2.5 m.

In order to characterize the near surface geology of the area, resistivity tomography was performed along a survey line parallel to the tunnel at a distance of approximately 20 m from it. The Schlumberger array with 2 m-electrode exhibits fine vertical resolution and is less influenced by 3D effects (Nyari, 2003).

The geoelectrical model (Fig. 1b) shows two layers, one being a high resistivity layer (conglomerate) and the other being a low resistivity layer (due to increased clay content). The conglomerate was excavated for the construction of the tunnel and the excavation material covered it. A sketch section at the test sites shows the tunnel and the above mentioned layers (Fig. 1c).

ANALYSIS OF GEOPHYSICAL METHODS

Resistivity tomography

The main aim of this experiment was the comparison of common resistivity arrays (Fig. 2a) employed for the detection of confined bodies. Resistivity tomography measurements were acquired over the tunnel located on the Campus of the Technical University of Athens by using the LUND-ABEM multi-electrode system. For the inversion, we choose the "RES2DINV" software (Loke and Barker, 1996). The survey lines were perpendicular to the tunnel and electrode distance was 1 m. The excavated area rather than the tunnel alone has influenced the measurements.

The forward and reversed Pole-Dipole arrays use the same distant current pole which is located offline. The measuring protocol (416

measurements) has $a=1, 2, 4, 6$ and $n > 2$. Both geoelectrical sections (Fig. 2b,c) exhibit lateral resistivity variations due to the presence of the excavation area and the underlying layer. Nevertheless, the more precise part of the image is that to the side of the current electrode.

The combined inversion of forward and reversed arrays generated an improved picture of the underground (Fig. 2d). If apparent resistivity measurements for potential dipole near the target are excluded, then the optimized section (Fig. 2e) accurately shows the interface of the overlying layer but it fails to image the edges of the excavation area.

The measuring protocol for the Schlumberger array excludes the Wenner values and has generally big " n " (351 measurements). The geoelectrical section (Fig. 2f), does not provide a clear indication of the top, bottom and side edges of the excavation area. This is probably due to the limited number of measurements and low sensitivity at these depths. Thus, this array does not delineate the target.

Two Dipole-Dipole arrays having either a current dipole on the left or the right part of the array employ a measuring protocol with $a=1, 2, 4, 6$ and an analogously increasing " n " (379 measurements). Both arrays (Fig. 2g, h) image the side edges and bottom of the excavation area. The interpretation of the average resistivity values from both arrays (Fig. 2i) after excluding noisy measurements (RMS more than 20%), gives a better, clearer and more detailed image. This procedure is very effective for Dipole-Dipole measurements exhibiting low signal to noise ratio.

The Pole-Pole array has a measuring protocol (335 measurements) with $a=3, 4, 5, 6, 8, 10, 12, 14, 16, 18, 20$, offering the greatest depth of investigation and the widest coverage. The geoelectrical section (Fig. 2j) images very well the excavation area, but it does not accurately image the top of the clay layer. Therefore, as far as the resolution of the specific measuring protocol is concerned, it is better near the surface. If measurements with $n=12, 14, 16, 18$ are excluded, the model (Fig. 2k) does not show the clay layer and the exact position of the target.

If the data sets from all arrays are inverted (inversion of combined data), the model (Fig. 2l) does not give a better picture of the underground. Although the combined model gives a more detailed picture as far as the target is concerned, it does not map the clay layer well.

A stacking technique is proposed which requires that the models for each array must be

created with the same interpolation parameters (grid size of x, z). An average value for every node of the grid is calculated using the corresponding resistivity values of the models from all arrays. The combined average model (Fig. 2m) gives a better image of both the excavation area and the underlying layer. This technique tends to “eliminate” the artifacts from the model.

Microgravity

A microgravity survey was carried out using a Lacoste Romberg model G gravity meter. The microgravity grid consists of 10 parallel lines 25 m in length with in-line spacing of 2 m. The direction of the lines is perpendicular to the tunnel. The station spacing was 0.5 m near the tunnel (at distances less than ± 2.5 m) and 1 m elsewhere (Fig. 3a).

Drift and diurnal corrections were made, using a fixed base station where readings were repeated approximately every 50 minutes. The base station was placed in a stable rocky area outside the survey grid far from the tunnel. We took at least 3 readings at every station. In general, the quality of measurements was good some stations, it was difficult to accurately place the metal plate and the gravimeter horizontally due to vegetation, trees and surface heterogeneities. In order to speed up the acquisition procedure, we took only one reading along the three last lines. The quality of measurements in these three lines was very poor

and, as a result, had to be excluded from the analysis. This unsuccessful attempt points out that one should never try to save acquisition time against accuracy of microgravity measurements.

Standard corrections such as free air, longitude and Bouguer were calculated using the elevation difference (dh) between the measuring station and the base station (an accuracy of 5 mm was achieved for elevation). The density was estimated ($\rho = 2.52 \text{ g/cm}^3$) by the Nettleton method.

Topographical corrections for A, B, C, D Hammer zones were also calculated using the digital topographic map of the survey area. Topography plays a negligible role for shallow targets and distances greater than 130 m. The map of topographical corrections follows the pattern of the local topography (Fig. 3b).

Due to the varying station spacing, data were firstly interpolated using a minimum curvature technique (1x2 m grid). A regional-residual separation (linear equation) followed by a low pass filter (moving average) enhanced the target’s anomaly by eliminating the high frequency noise (Fig. 4a). Admittedly, it is not so easy to delineate the buried tunnel from the unprocessed residual map. On the other hand, it is obvious that there is a characteristic low gravity zone in the filtered map, indicating the presence of the excavation area and the buried tunnel. This can also be seen in the Fourier domain (Fig. 4b).

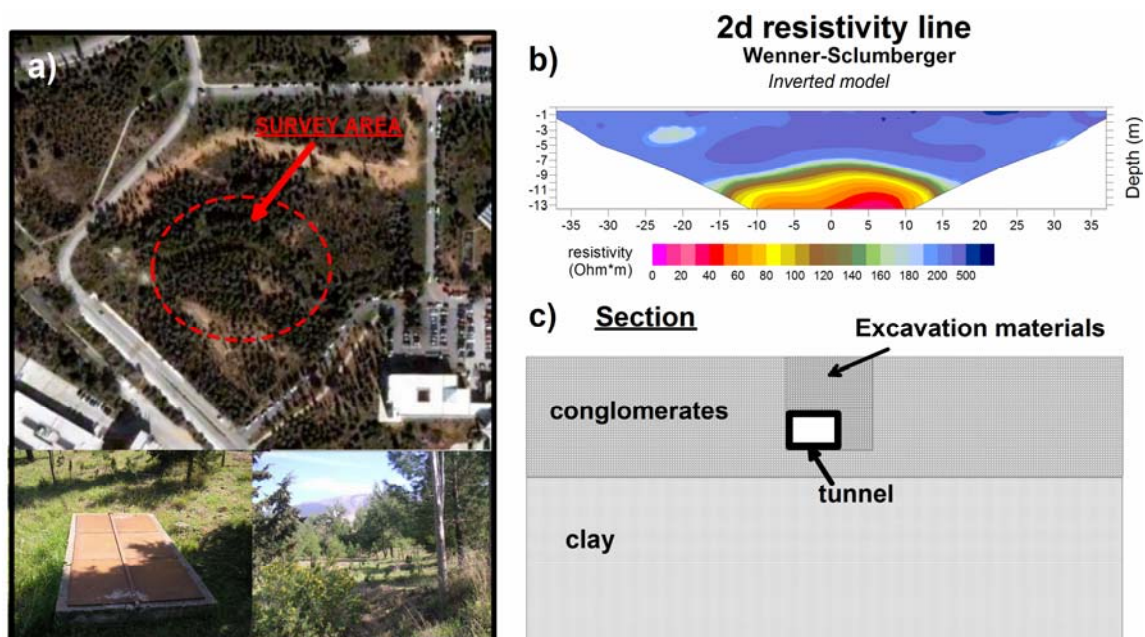


FIG. 1. a) Perspective images of survey area, b) Resistivity section parallel to the tunnel in order to detect the near surface geology of the area, c) Sketch of the section of the area under investigation.

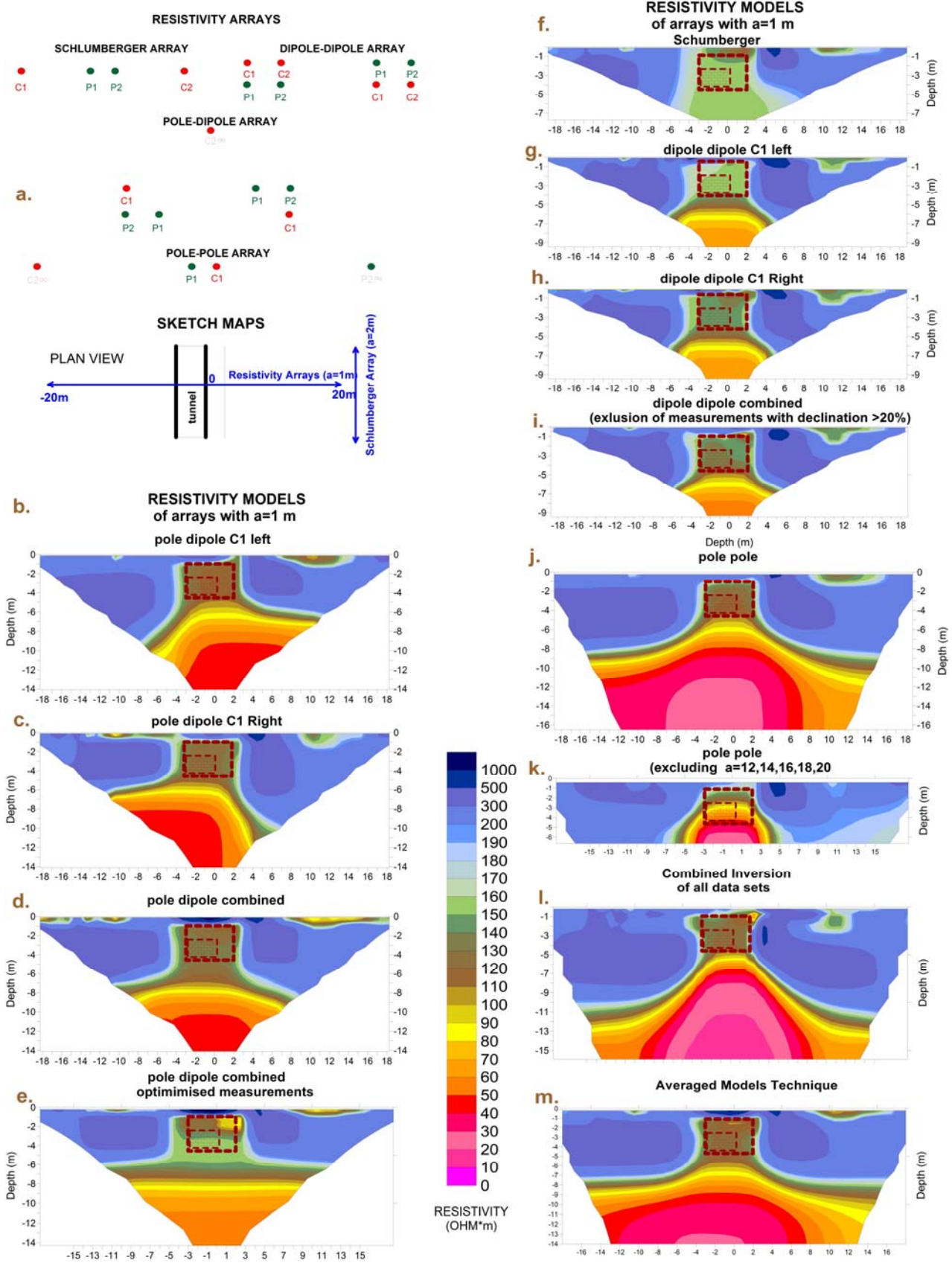


FIG. 2. a) Electrode position of resistivity arrays and plan view of a sketch map of the area under investigation. b, c, d, e, f, g, h, i, j, k, l, m) Resistivity sections (RMS error <3%) for various resistivity arrays. The survey line is perpendicular to the tunnel. The excavation area including the tunnel is outlined.

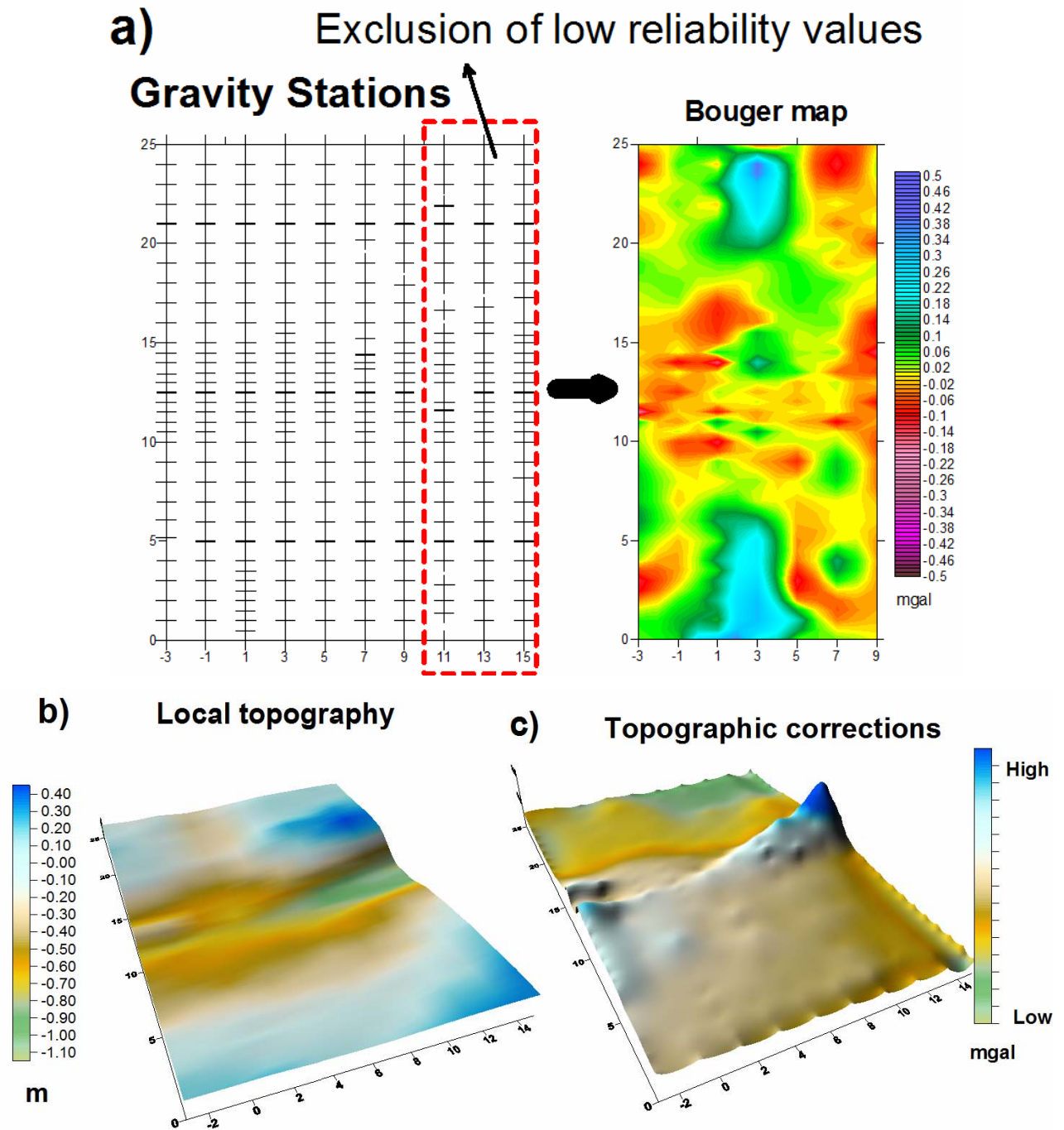


FIG. 3. a) Microgravity station and Bouger map, b) Comparison of local topography with topographic corrections.

As an additional step, we inverted the residual filtered data using the Grablox software (Pirttijärvi and Elo, 2006). This software is mainly used for large scale gravity surveys but it can be used in microgravity surveys as well (Elo, 2006). The inversion method estimates the density of each block by minimizing the difference between the measured and the computed gravity data. The linearized inversion uses the singular value decomposition (SVD) technique with adaptive

damping (Pirttijarvi, 2009). Using the available information from the resistivity method, it was possible to optimize the inversion parameters (size of cells and depth of the model) and to reduce the number of acceptable gravity models. The model defines the limits of the target. Figure 4c shows the density distribution for cross section A-B. Moreover, a 3D image shows only the low density values and gives the 3D perspective view of the tunnel (Fig. 4d).

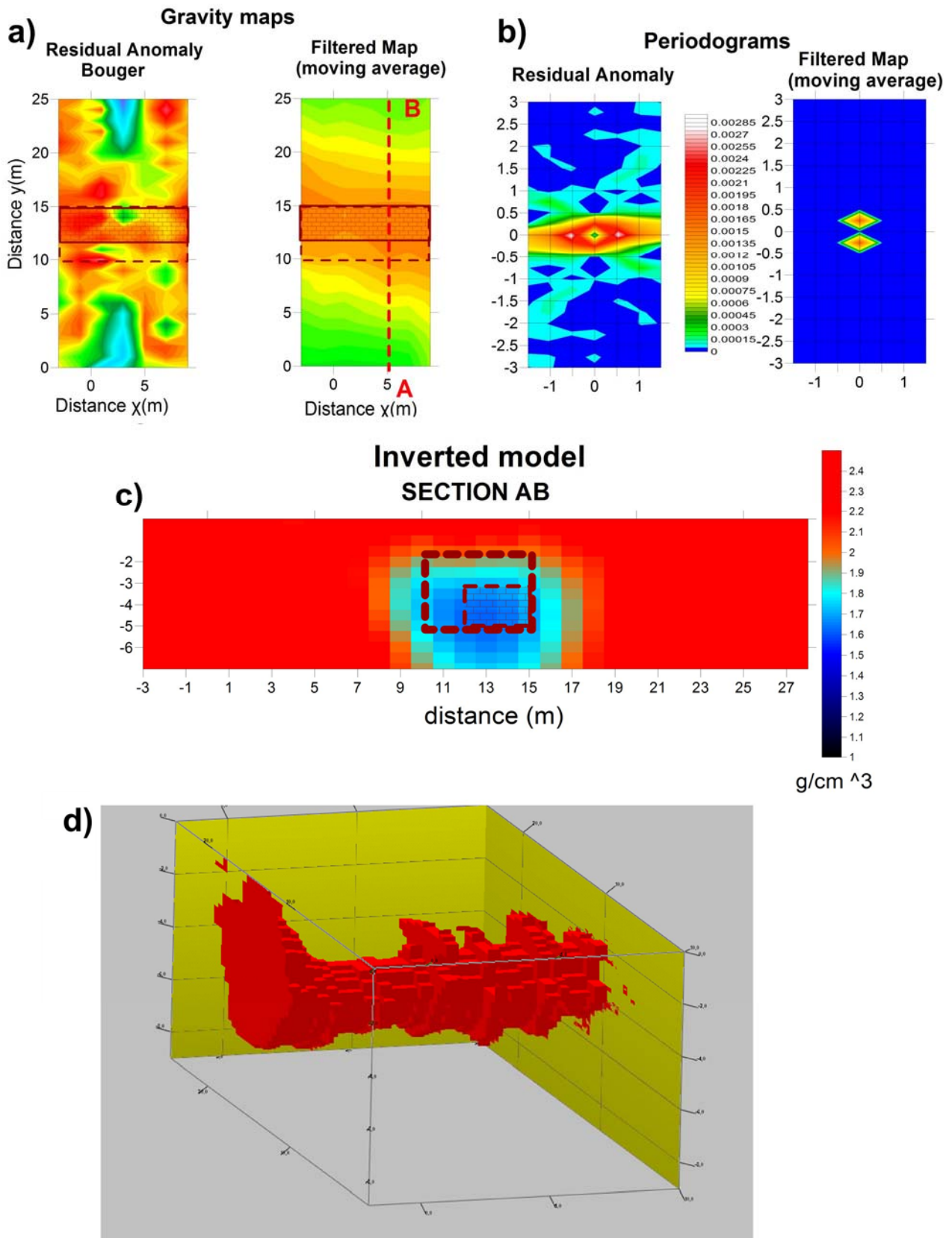


FIG. 4. a) Residual and filtered gravity map, b) Periodograms of residual and filtered gravity map, c) Density distribution as a function of depth of section AB, d) a 3D perspective image showing only the low density values, delineating the direction of the tunnel.

Multichannel Analysis of Surface Waves (M.A.S.W.)

Measurements were carried out along a survey line (Fig. 5a) whose direction is perpendicular to the tunnel using the roll along technique (Xia et. al, 2000). The acquisition parameters were selected by taking into account both the target's dimension and the maximum desirable depth (10-12 m). Thus, 24 geophones of 4.5 Hz frequency were used with receiver spacing of 1 m. A 5 kg sledge hammer was utilised with a minimum source-receiver offset of 2 m. The main acquisition parameters are presented in Table 1.

TABLE 1. Acquisition parameters of M.A.S.W. measurements.

Recorder	SmartSeis (Geometrics)
Geophones	24 / 4.5 Hz / Vertical comp.
Seismic source	Sledge hammer 5 kg
Sampling rate	1.0 ms
Record length	1024 ms

Firstly, the specific configuration of the 24 geophones was laid far away from the tunnel. The vertical stacking technique was used for every shot in order to increase signal to noise ratio. Once the data collection was completed, SeisImagerTM software was used to calculate phase velocities of the ground roll (dispersion curves) for each shot gather. Then, inversion was performed on each dispersion curve to generate an S-wave velocity versus depth profile (Fig. 5b).

Figure 5c represents a perspective view of phase velocity maps (Luke et al., 2008). An interesting point is that there is an increase in higher mode energy for the shot gathers near the target.

Nevertheless, only the fundamental mode of the surface waves was inverted by employing phase velocities at frequencies ranging from 20 to 35 Hz. The initial model consisted of 15 horizontal layers with a maximum depth of 12 m. The pseudo-section of S-wave velocity (Fig. 5d) is the outcome of interpolating (krigging method) the 1D velocity profiles. This image of S-wave velocity distribution shows three distinct zones: a) a low velocity anomaly ($V_s < 500$ m/s) corresponding to the excavation area and the tunnel, b) a surface layer of average $V_s=550$ m/s and 6.5 to 7 m thickness and c) an underlying layer of average $V_s=650$ m/s. Although the method detected the target, the V_s pseudo-section does not define the

target limits. Such images should be interpreted keeping in mind that the length of the configuration and the moving step play an important role in lateral resolution.

An additional procedure involves the analysis of the data in the frequency domain. A study of the effect of lateral inhomogeneities on the propagation of Rayleigh waves in an elastic medium (Nasseri, 2006) shows that a void interacts with the Rayleigh wave and entrapped energy is observed at regions over the void. The degree of this interaction depends on the size and the depth of the void and the frequency content of the incident wave.

In order to observe the effect of the buried tunnel in the frequency domain, two specific shot gathers were chosen for analysis. The first shot (Line 1) is far from the target and the second one (Line 8) is above the target. The normalized power spectrum remains the same for all the traces belonging to the first shot (Fig. 6a). The second shot (Fig. 6b), where the target is under the center of the receiver array, exhibits in the normalized power spectrum higher energy for traces recorded on top of the target. This is also observed in shot gathers where the target is under the edge of the receiver array.

Magnetics

The magnetic data grid covered a 25x22 m area. It consists of 23 parallel lines with a station interval of 0.5 m and an inline distance of 1 m (Fig. 7a). The total magnetic field was measured (Geometrics G-856 proton magnetometer) simultaneously at two height levels of every station using two sensors (the gradient method). The lower sensor height was 0.70 m and the upper sensor was 1.4 m higher (Fig. 7b). Despite the fact that there was no need to use a base station for diurnal corrections (the gradient method), a base station was used for single sensor data processing.

The data from both sensors were corrected for diurnal variations. Maps of the magnetic intensity and its vertical gradient were generated using the minimum curvature interpolation technique (Fig. 7c). An area of low magnetic intensity values is visible in the north, north-east part of all maps in contrast to an area of high magnetic intensity values in the south, south-west part. These two zones constitute a characteristic magnetic dipole, suggesting the presence of a body with high magnetic susceptibility. The tunnel lies approximately between these zones. This magnetic anomaly is due to the presence of the

reinforcement and cables in the tunnel, rather than due to the void itself. Moreover, other higher frequency anomalies appear in the maps, having greater intensity in the lower sensor and the gradient maps. For the better definition of the tunnel limits, various processing methods were

used (first direction derivative, reduction to the pole, shade relief maps). The shaded relief maps (shading method: Lambertian reflection, light position angle: horizontal 90, vertical 25 - Figure 7d) delineate the target with great accuracy.

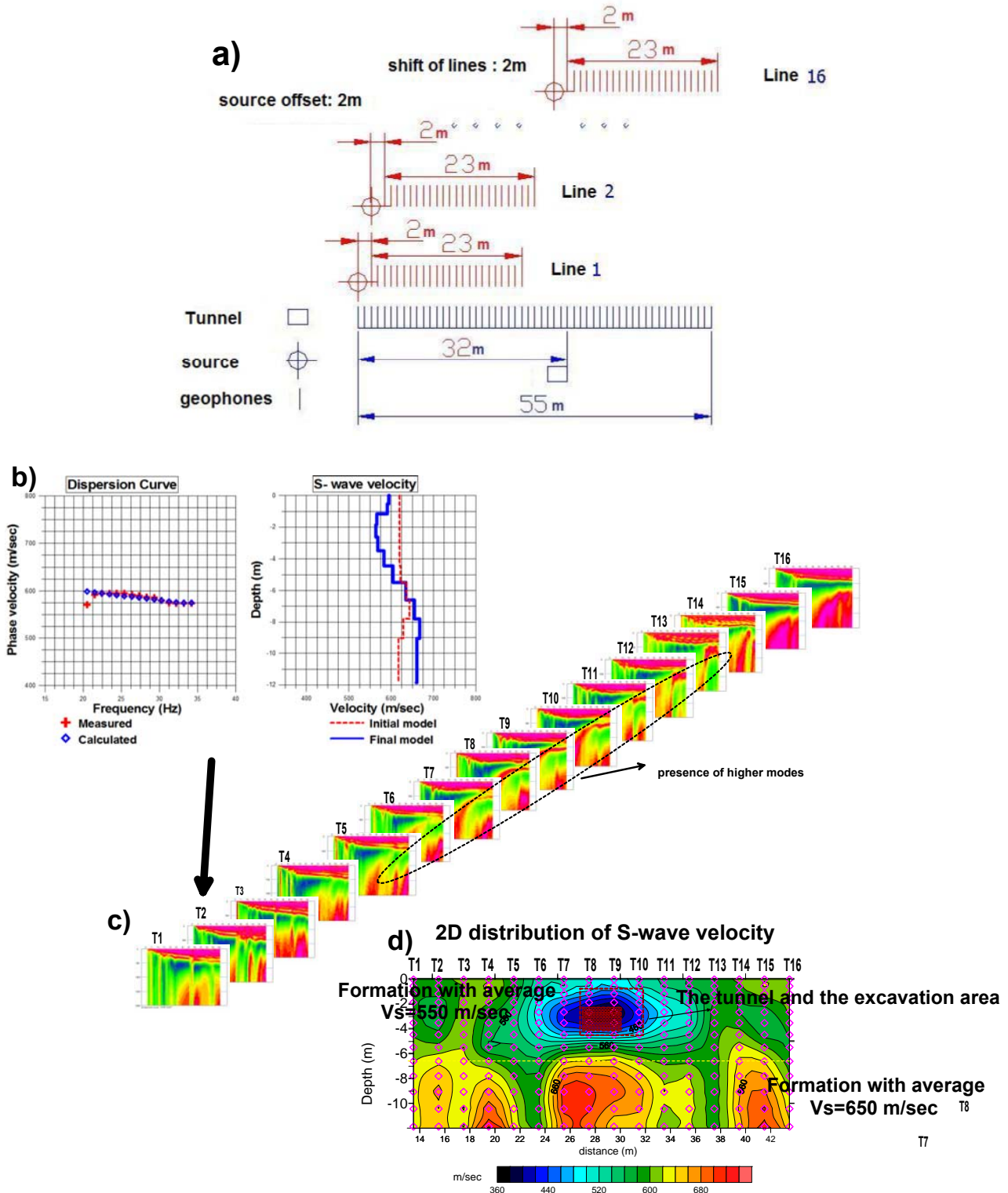


FIG. 5. a) Sketch of MASW measurements using roll along technique, b) Dispersion curves and model of line 2 (T2), c) perspective view of phase velocity maps showing an increase in higher modes near the tunnel, d) S-wave velocity pseudo-section.

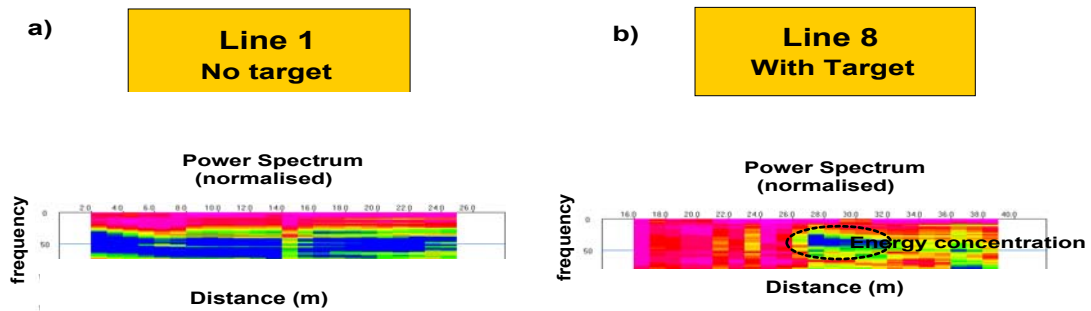


FIG. 6. Shot gathers in frequency-distance domain for: a) Line 1 (no target) and b) Line 8 (on top of the target). Color scale is the same.

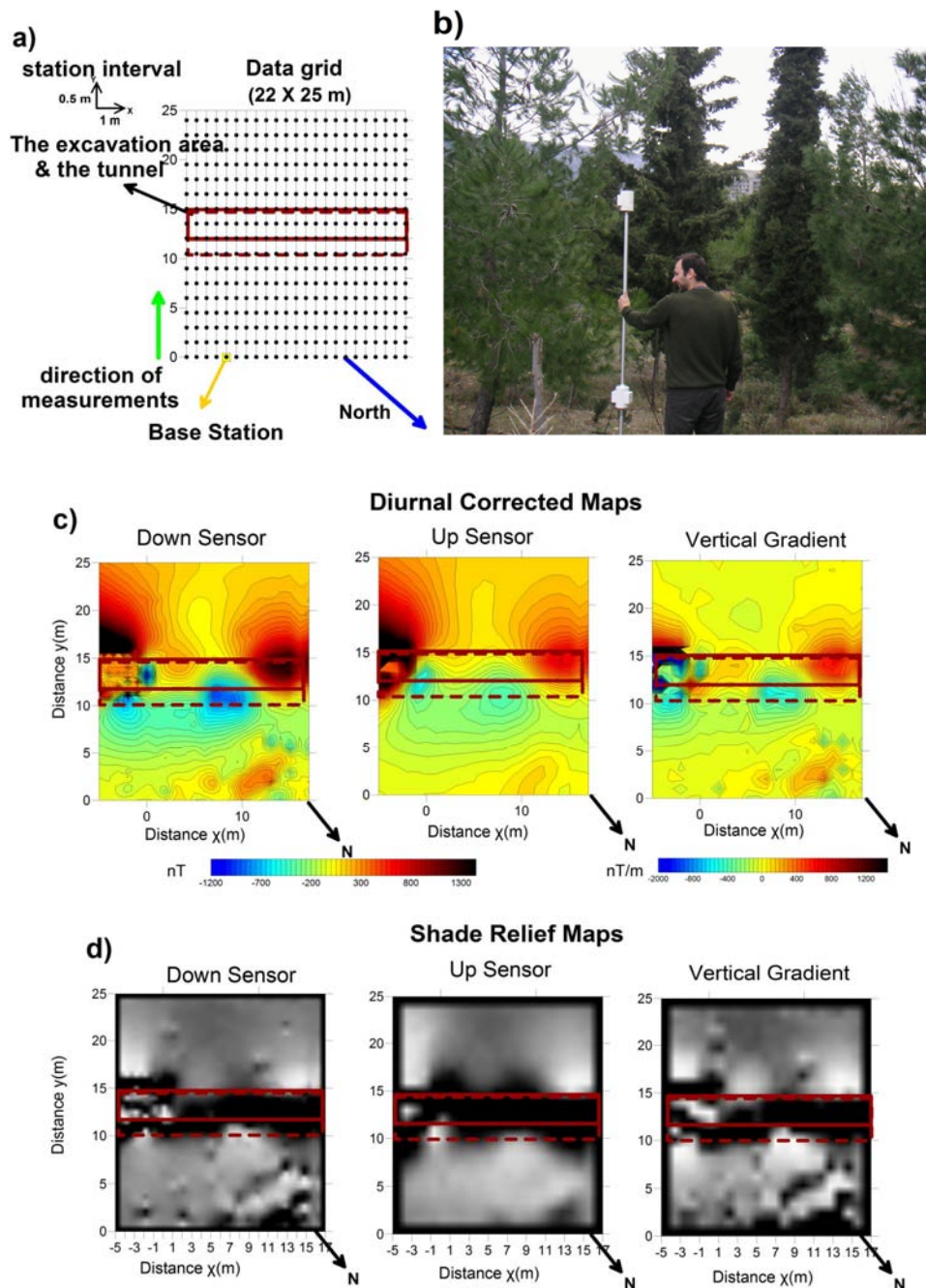


FIG. 7. a) Grid of magnetic measurements, b) magnetic measurements carried out with two sensors in different heights (gradient method), c) diurnal corrected maps of lower, upper sensor and vertical gradient, d) shade relief maps lower and upper sensor and vertical gradient.

CONCLUSIONS

This study involves the application and the analysis of four geophysical methods (resistivity tomography, microgravity, magnetic, M.A.S.W.) for the detection of a target under controlled site conditions.

Resistivity tomography, with moderate acquisition time, gives information both for the target and the near surface geological formations. Dipole-Dipole and Pole-Dipole are the most suitable arrays for tunnel detection. If both forward and reversed measurements using the Pole-Dipole array are combined, the inversion of these data provides improved images of the underground. The Pole-Pole array produces a model with good lateral resolution, great depth and wide coverage. Wenner-Schlumberger is classified as having low target detection ability compared to the other arrays. The sensitivity and the signal to noise ratio constitute the basic factors for an optimum protocol design.

The success of the microgravity method greatly depends on following the proper field procedures with care as well as on the processing steps (low pass filters, directional derivatives etc.). Prior information is necessary for the inversion of the microgravity data. The density distribution model can be directly compared to the sections provided by other geophysical methods.

The Multi-channel Analysis of Surface Waves (using the roll along technique) with moderate acquisition time images lateral heterogeneities and the layering. However, the final image appeared to be smoothed, presenting low resolution. An additional procedure for the detection of underground confined bodies is presented which involves power spectra comparison. Traces of the shot gather exhibiting higher power spectrum values indicate the location of a void.

The magnetic method and especially the gradient method requiring low acquisition time and simple field procedures, accurately delineates the tunnel due to the increased magnetic susceptibility contrast between the target and the host rock. On the other hand, the information for near surface geology is almost negligible.

If there is a confined body to be detected, an integrated geophysical approach should be followed. Even in a near surface application, factors such as the site and the target characteristics (geology, man made or physical void, size and depth) make it difficult to choose a single optimum method. The acquisition strategy, the processing steps and the interpretation of the

data play a vital role in the quality and reliability of each geophysical method.

REFERENCES

- Branston, M., W., and Styles, P., 2006, Site characterization and assessment using the microgravity technique: a case history, *Near Surface Geophysics*, 4, p. 377-385.
- Butler, D., K., 1980, Microgravimetric techniques for geotechnical applications, *Miscellaneous Paper GL-80-13: U.S. Army Engineer Waterways Experiment Station, Vicksburg, MS*, 121 pp.
- Butler, D., K., 1984, Microgravimetric and gravity gradient techniques for detection of subsurface cavities, *Geophysics*, 49, p. 1084-1096.
- Elo, S., 2006, Progress and Problems in Near Surface Gravity, 12th European Meeting of Environmental and Engineering Geophysics, Helsinki, Finland, Extended Abstracts, P014.
- Hinze, 1990, The role of gravity and magnetic methods in engineering and environmental studies, *Geotechnical and Environmental Geophysics: Investigations in Geophysics, SEG, No 5, Vol. 1*, p. 75-126.
- Johnson, W., J., 2003, Case Histories of DC resistivity measurements to map shallow coal mine workings, *The Leading Edge*, 22, p. 571-573.
- Kaufmann, R., D., and DeHan, R., S., 2007, Microgravity Mapping of Karst Conduits within the Woodville Karst Plain of North Florida, *Symposium on the Application of Geophysics to Engineering and Environmental Problems (SAGEEP '07)*, Denver, Colorado, SAGEEP, Vol. 20, p. 1517-1526.
- Ki, L., and Szabo, Z., 2005, Microgravimetric investigations for shallow depth cavity detection, 11th European Meeting of Environmental and Engineering Geophysics, Palermo, Italy, Extended Abstracts, P025.
- Loke, M., H., and Barker, R., D., 1996, Rapid least-squares inversion of apparent resistivity pseudosections by a quasi-Newton method, *Geophysical Prospecting*, 44, p. 131-152.
- Luke, B., and Calderon-Macias, C., 2008, Scattering of surface waves due to shallow heterogeneities, *SEG Annual Meeting, Las Vegas*.
- Nasseri, A., 2006, Study of the effect of lateral inhomogeneities on the propagation of Rayleigh waves in an elastic medium, PhD thesis, Waterloo, Ontario, Canada.
- Nyari, Z., 2003, Problems of detecting buried 3D objects with 2D geoelectric profiling methods, 65th EAGE Conference & Exhibition, Stavanger, Norway, Extended Abstracts.
- Orfanos, C., Apostolopoulos G., Amolochitis, G., and Leontarakis, K., 2008, Integrated Geophysical Approach for the Detection of Underground Voids in a Construction Site, 70th EAGE

- Conference & Exhibition, Rome, Italy, Extended Abstracts, P097.
- Pirttijärvi, M., and Elo, S., 2006, Constrained inversion of gravity data, Bulletin of the Geological Society of Finland, special issue 1, p. 124.
- Pirttijärvi, M., 2009, GRABLOX2: Gravity interpretation and modelling software based on 3-D block models, User's guide, version 2.0, University of Oulu, Department of Physics.
- Rybakov, M., and Rotstein, Y., 2005, Cave detection near the Dead Sea—a micromagnetic feasibility study, The Leading Edge, V. 24, no. 6, p. 585-590.
- Sheets, R., A., and Munk, J., 1997, Detection of underground voids in Ohio by use of geophysical methods, U.S. Geological Survey Water-Resources Investigations, Report 97-4221.
- Styles, P., Toon, S., Thomas, E., and Skittrall, M., 2006, Microgravity as a tool for the detection, characterization and prediction of geohazard posed by abandoned mining cavities, First Break, 24, p. 51-60.
- Xia, J., Miller, R., D., Park, C., B., and Ivanov, J., 2000, Construction of 2-D vertical shear-wave velocity field by the Multichannel Analysis of Surface Wave technique, Symposium on the Application of Geophysics to Engineering and Environmental Problems, Arlington, Va., February 20-24, p. 1197-1206.
- Yule, D., E., Sharp, M., K. and Butler, D., K., 1997, Microgravity investigations of foundation conditions. Geophysics, 63, p. 95-103